Observable regularization of two-phase flows and reacting flows

By B. Aboulhasanzadeh† AND K. Mohseni†

Inviscid fluid problems are prone to the developing high-wave-number irregularities. An evaluation of the observable Euler equations (Mohseni 2009) for regularizing two-phase flows and reacting flows are presented. Observable Euler and Navier-Stokes equations are derived from the conservation laws with a consideration of the observability limit of any field quantity before the derivation of the governing equations. As a result, regularization of the governing equations is done at the level of the partial differential equations before any numerical discretization. An LES form of the observable equations is presented in order to show the observable subgrid scales. Besides the observable conservation laws for mass, momentum, and energy, in two-phase flows we derive the observable volume fraction equation. All the numerical simulations are performed by a pseudo-spectral method to avoid introduction of numerical dissipation. We present the result of a shock-bubble interaction for two-phase flows. We also present the numerical simulation of observable Euler equations for one-dimensional reacting flows.

1. Introduction

Chemically reacting flows are essential in many engineering applications, including internal combustion engines, jet engines, and explosive devices, among others. While a large amount of theoretical and numerical effort has gone into understanding these kind of flows in the past century, it is not until recently that researchers have the computational capability to solve detailed simulations of these types of flows (Lv & Ihme 2014; Moin & Apte 2006). Even without chemical reactions, fluid flows usually contain nonlinearities that might create numerical challenges. Examples include shocks, turbulence, and material interfaces. Chemical reactions add another level of complexity and new challenges to the problem. Many numerical methods have been developed over the past three decades to deal with these problems; however, these challenges are considered to be separate issues and are dealt with separately in different communities. We postulate that all these issues are a manifestation of what we call k_∞, or high-wave-number irregularity.

An implicit assumption in the continuum governing equations for any fluid flow is that field quantities have infinite resolution. This contradicts any experimental measurement, which always has a limiting resolution, or any numerical computation, which always has a minimum computational cell size. While the size of this limiting scale could be progressively reduced, it could never be zero. This points to a limited observability of any field quantity. When one looks at the the governing equations in the Fourier domain, the nonlinear advective term can be a mechanism for generating higher wave modes from lower wave modes. As a result, any smooth initial condition could constantly generate higher wave modes so that there will not be enough resolution to correctly capture the highest wave numbers, or what we call k_∞ irregularity. This results in numerical issues

† Department of Mechanical & Aerospace Engineering, University of Florida

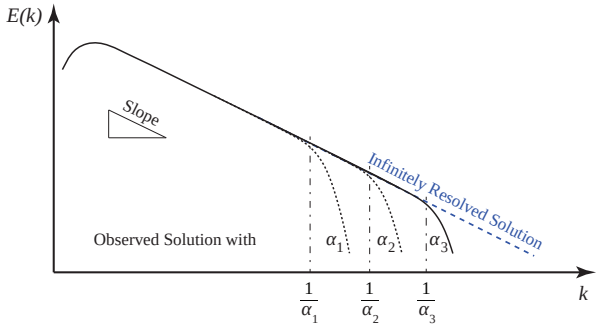

FIGURE 1. Schematic of the energy cascade from low wave modes to higher wave modes is shown for an infinitely resolved field quantity, e.g., $u^2/2$ for the inviscid Burgers' equation, (dashed line) and an observed solution, e.g., $\overline{u}^2/2$ for the regularized Burgers' equation, with different limits of observability $\alpha_1 > \alpha_2 > \alpha_3$ (black dotted lines). The slope of the resolved part of the one-dimensional Burgers' equation is equal to -2.

that are usually handled by adding some sort of numerical viscosity (Lantz 1971) or hyperviscosity (Cook & Cabot 2005) to regions with a high gradient of flow variables. We hypothesize that another way to resolve these issues is to address them at the level of derivation of the governing partial differential equations (PDEs) before any discretization is implemented. To this end, one must adhere to the observability limit of any field quantities while deriving the governing PDEs.

By introducing the limited observability assumption into the derivation of the divergence theorem, an observable divergence theorem could be derived (Mohseni 2010). With this theorem one can use any conservation law to derive the observable conservation equation. A conjecture is that the observable equations have better regularity properties and they could avoid k_∞ irregularity at a PDE level before any discretization is applied. With this strategy we have been able to derive the observable Euler and observable Navier-Stokes equations to solve many single-phase benchmark problems containing shocks and turbulence. In all of these tests, the observable results were comparable to or better than the benchmark results for the Euler or Navier-Stokes equations available in the literature. With the past success of this method, we extend the observable method to the solution of two-phase flows and reacting flows. An LES form of the observable equations is presented to show the observable subgrid scale. An advantage of the observable equation could be its unified form of the subgrid-scale terms for problems involving shock, turbulence, sharp interfaces and chemical reactions. In this study we develop and evaluate these equations for simulating flows with shocks, sharp interfaces, and chemical reactions. In Section 2 the concept of observability is presented. Then results for shock-bubble interactions are presented in Section 3.1, and the results for a one-dimensional detonation problem are presented in Section 3.2. Finally, the concluding remarks and future directions are presented in Section 4.

2. Observability limit of field quantities and its consequences

Solving fluid dynamics equations often requires special care in treating the nonlinear advection term, e.g., $u\cdot\nabla u$. In the absence of any localized diffusion process, this nonlinear term can create discontinuities in the flow field even when starting from a smooth initial condition. Traditionally, the computational challenges of simulating multiphase flows,

shocks, and turbulence are viewed as separate problems. However, if these problems are studied closely in the Fourier domain, all these challenges arise from a nonvanishing tail in the Fourier domain, what we refer to as k_∞ irregularity. To put this into context, consider the Burgers' equation, $u_t + uu_x = 0$, with a smooth initial condition, $u = \sin(x)$ within $x \in [0, 2\pi)$. Initially, u can be represented with a single Fourier mode. The nonlinear term uu_x represents a convolution in the Fourier space, which means that at each time step the solution's maximum wave number with a nonzero Fourier coefficient is doubled. In theory, with infinite resolution, the tail of spectral energy continues with a slope of -2 (in one dimension) as the wave number, k, goes to infinity (Gurbatov *et al.* 1997; Kraichnan 1968) (see Figure 1). However, in a finite time, the number of available modes in the solution, m, will be larger than the available number of modes in any computational simulation, n, as a result of finite resolution. A similar continuous high-wave-number problem exists in inviscid flows with sharp interfaces, turbulence or reacting flows. We believe all these are manifestation of the k_∞ irregularity.

As a way around this difficulty, Norgard & Mohseni (2008, 2009) regularized the inviscid Burgers' equation by advecting u with $\overline{u}$, resulting in a Hamiltonian equation $u_t + \overline{u}u_x = 0$. Here, u is the fully resolved field quantity and $\overline{u}$ is the corresponding averaged field quantity. The barred quantities are calculated with a convolution given by

$$\overline{f} = g^\alpha * f. \tag{2.1}$$

Here, g^α is an averaging kernel with an averaging length scale α, which is the observability scale for the equations. This observability limit is the length scale below which the Fourier tail of the barred field quantity drops at a faster rate than the infinitely resolved field quantity. See in Figure 1 the spectral energy for the observed solution using different observability limits, where $\alpha_1 > \alpha_2 > \alpha_3$. g^α can be any normalized ($\int g^\alpha = 1$), non-negative ($g^\alpha \geq 0$), decreasing ($|x_1| \geq |x_2| \Rightarrow g^\alpha(x_1) \geq g^\alpha(x_2)$), and symmetric ($|x_1| = |x_2| \Rightarrow g^\alpha(x_1) = g^\alpha(x_2)$) convolution kernel (Norgard & Mohseni 2008). Norgard & Mohseni (2009) proved the existence and uniqueness of the solution and its convergence to the weak solution of multidimensional Burgers' equation as $\alpha \to 0$ for a subset of filters with the form $\hat{g}(k) = 1/(1 + \sum_{j=1}^{N} C_j k^{2j})$; a hat represents the Fourier transform of a quantity and C_j is the filter constant. Note that as $\alpha \to 0$, by definition in Eq. (2.1), the regular Euler and Navier-Stokes equations can be obtained from the observable equations.

Both the Euler and Navier-Stokes equations are derived from infinitely resolved field quantities, which means the field quantities are assumed to be fully observed, whether experimentally or computationally, no matter how small the observability length scales are (limit of α, $\Delta x \to 0$). Norgard & Mohseni developed the regularization of the Euler set of equations using similar ideas that they used for the Burgers equation and proved the convergence to the weak solution of Euler equations (Norgard & Mohseni 2010). Mohseni (2010) developed the observable divergence theorem and derived the observable Euler equations from the conservation laws.

Observability limit has a direct impact on some of the integral theorems of calculus, the derivation of which is based on the assumption of infinite observability of field quantities. For example for a nonlinear vector field, $\mathbf{F} = \mathbf{fV}$, one can define the observable divergence, *odiv* (see Mohseni 2009), using

$$odiv\,\mathbf{F} = \overline{\mathbf{f}}\nabla \cdot \mathbf{V} + \overline{\mathbf{V}} \cdot \nabla \mathbf{f}. \tag{2.2}$$

The observable divergence theorem for a region of space Ω with a surface boundary S

states that

$$\iiint_\Omega o div\,\mathbf{F}dV = \iiint_\Omega \left(\overline{f}\nabla\cdot\mathbf{V} + \overline{\mathbf{V}}\cdot\nabla f\right)dV = \iint_S \mathbf{F}\cdot\mathbf{ndS}, \tag{2.3}$$

where $\mathbf{n}$ is the normal vector to the surface. In the limit of infinite observability where $\alpha \to 0$, one recovers the divergence theorem of Gauss, $\iiint_\Omega div\,\mathbf{F}dV = \iint_S \mathbf{F}\cdot\mathbf{n}dS$. In the following section, the observable conservation equations are presented first. We then present and validate an observable volume fraction equation for capturing the material interface and defining material properties inside each phase.

3. Observable solution for two-phase and reacting flow

Starting from the successful experience from the observable solution for a single-phase flow we first extend the method to two-phase flow and then present a solution for reacting flows for a one-dimensional detonation problem. These are the initial steps for a unified observable formulation for two-phase reacting flow. In the following subsections we present first the equations for the solution of shock-interface interaction and then the equations and the results for the detonation problem.

3.1. *Shock-interface interaction*

In order to simulate a shock-interface interaction, we use the observable Euler equations (Mohseni 2009)

$$\frac{\partial\rho}{\partial t} + \overline{\rho}\nabla\cdot\mathbf{u} + \overline{\mathbf{u}}\cdot\nabla\rho = 0, \tag{3.1}$$

$$\frac{\partial\rho\mathbf{u}}{\partial t} + \overline{\rho\mathbf{u}}\,\nabla\cdot\mathbf{u} + \overline{\mathbf{u}}\cdot\nabla\rho\mathbf{u} + \nabla p = 0, \tag{3.2}$$

$$\frac{\partial\rho E}{\partial t} + \overline{\rho E}\nabla\cdot\mathbf{u} + \overline{\mathbf{u}}\cdot\nabla\rho E + \overline{p}\nabla\cdot\mathbf{u} + \overline{\mathbf{u}}\cdot\nabla p = 0 \tag{3.3}$$

for the mixture quantities, with the assumption that coexisting phases reach instantaneous equilibrium, $\mathbf{u} = \mathbf{u_1} = \mathbf{u_2}$ and $p = p_1 = p_2$, where subscripts 1 and 2 refer to phases 1 and 2, respectively. The mixture quantities are defined by $\rho = \rho_1 z_1 + \rho_2 z_2$ and $\rho E = \rho_1 E_1 z_1 + \rho_2 E_2 z_2$, where z_1 and z_2 are the volume fractions of phases 1 and 2 and $z_1 + z_2 = 1$. For the sake of simplicity, we consider a gas-gas problem for which the ideal gas equation of state is a good approximation, i.e., $\rho E - \rho\mathbf{u^2}/2 = \Gamma p$, with $\Gamma = 1/(\gamma-1)$. Here, γ is the ratio of specific heat of material at constant pressure to its specific heat at constant volume. The mixture Γ is defined as $\Gamma = 1/(\gamma-1) = z_1/(\gamma_1-1) + z_2/(\gamma_2-1)$. An LES form of Eqs. (3.1)–(3.3) can be derived using the definition of the convolution kernel; for example, using a Helmholtz kernel in one dimension one obtains

$$\begin{aligned}
\overline{\rho}_t + \left(\overline{\rho\,u}\right)_x &= -3\alpha^2\overline{\left(\overline{u}_x\overline{\rho}_x\right)}_x,\\
\overline{\rho u}_t + \left(\overline{\rho u\,u} + \overline{P}\right)_x &= -3\alpha^2\overline{\left(\overline{u}_x\overline{\rho u}_x\right)}_x,\\
\overline{\rho E}_t + \left(\overline{\rho E}\,\overline{u} + \overline{u}\overline{P}\right)_x &= -3\alpha^2\overline{\left[\overline{u}_x\left(\overline{\rho E} + \overline{P}\right)_x\right]}_x,
\end{aligned} \tag{3.4}$$

which shows the unified form of the subgrid-scale terms in the observable equations.

In addition to the governing equation for the mixture quantities, we derived an equation for evolving the interface. For the purpose of capturing the interface while keeping pressure equilibrium at the interface, we considered the case of an interface-only problem, following Shyue (1998), in which velocity and pressure are constant in the domain

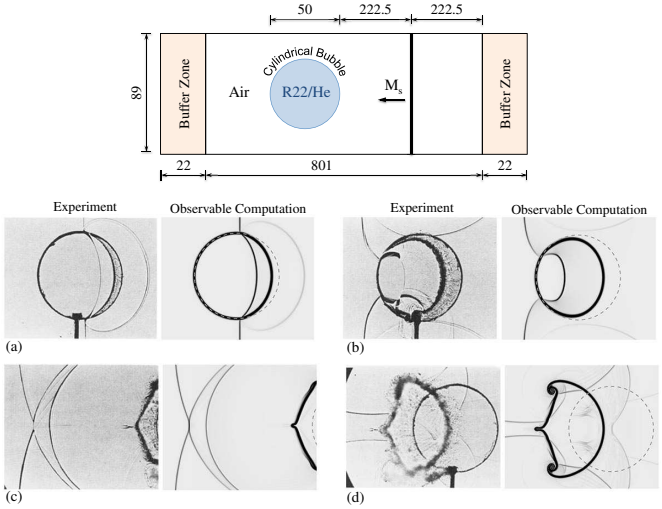

FIGURE 2. Schematic of a shock-bubble interaction problem setup and schlieren snapshots of the interaction of a planar $M_s = 1.22$ shock in air with a cylindrical Refrigerant 22 (R22) bubble at times (a) 55 μs, (b) 247 μs, (c) 318 μs, and (d) 417 μs. All units in the schematic are in millimeter. Experimental snapshots are from Haas & Sturtevant (1987).

while density and material properties change across the interface. Writing the observable conservation equations in terms of density ρ, velocity u, and internal energy ρe and simplifying them for the isolated interface problem, we derived the observable equation for the evolution of volume fraction

$$\frac{\partial z_1}{\partial t} + \overline{\mathbf{u}} \cdot \nabla z_1 = 0. \tag{3.5}$$

The governing equations are solved by a pseudo-spectral method for calculating spatial derivatives. As shown in Figure 2, a buffer zone is used on the left and right sides of the domain to make the computational domain periodic and avoid wave reflection from boundaries. For the time integration, a third-order TVD Runge-Kutta method is used (Gottlieb & Shu 1998). For dealiasing, a low-pass exponential filter, $G(k) = \exp(-36|k/k_{\max}|^{36})$, is used (Hou & Li 2007). For all initial conditions double filtering is used as explained in Norgard & Mohseni (2010). The problem setup is shown in Figure 2.

The problem studied here is a two-dimensional shock-bubble interaction in which a Mach 1.22 shockwave in air interacts with a cylindrical Refrigerant 22 (R22) bubble with $\gamma = 1.249$ and $\rho_{R22} = 3.712\,\mathrm{kg/m^3}$. We compare our observable result with the experimental result by Haas & Sturtevant (1987). A grid resolution of $\Delta x = 222\,\mu$m and a nondimensional observability limit $\alpha/\Delta x = 1$ are used here.

Figure 2 shows experimental schlieren images of a shock-cylindrical bubble interaction from Haas & Sturtevant (1987) in addition to numerical schlieren from our observable results. The incident shock hits the interface at $t = 0\,\mu$s; a shock wave reflects from the interface and another one refracts into bubble. Since the speed of sound is lower inside the bubble, the refracted shock moves with a lower speed compared with the incident shock outside the bubble. As a result the shock converges toward the end of bubble (see Figure 2(a)). The shock initially reflected from the interface reflects from the top and bottom walls and interacts with the bubble.

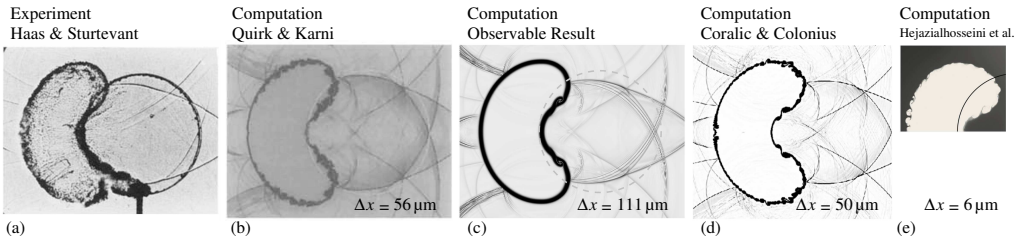

FIGURE 3. The result of a Mach 1.22 shockwave in air interacting with a cylindrical helium bubble. (a) Experimental schlieren at $t = 245\,\mu s$ from Haas & Sturtevant (1987). Panels (b), (c), and (d) are numerical schlieren images from the simulations by Quirk & Karni (1996), the observable method (our method), and Coralic & Colonius (2014), respectively. Panel (e) is a very similar simulation reported by Hejazialhosseini *et al.* (2010). Δx is the spatial resolution used for the computation.

The incident shock diffracted around the bubble arrives at the downstream edge of the bubble faster than the refracted shock. When the refracted shock, which is focused at the downstream edge of the bubble, hits the interface, it pushes the interface toward the downstream and creates a jet at that point (see Figure 2(c)). Then the refracted shock transmits into the air, trailing the defracted wave (Figure 2(c)). Interaction of the shock with the interface creates rollup and instability of the interface, which become visible in Figure 2(d). As seen in Figure 2, the observable method regularizes the equations and the results are in good agreement with the experiment.

The results in Figure 2 show good agreement between experimental and simulation snapshots. All the main waves and interfaces are captured correctly. Also, quantitative comparison for the speed of all the major waves shows that the observable results agree with the experimental results with less than 3% error, well within the range of 10% error, which is associated with the experimental results,

A comparison of the results of two-phase observable Euler equations and the available results from the literature showed that the observable method produces results with similar accuracy to other methods with an order of magnitude lower computational cost for two-dimensional simulation (see Figure 3). Note that by increasing resolution in the Euler equation, since the tail of the energy spectrum goes to infinity, there will be no convergence. As the resolution for Euler numerical solutions increases, we expect to see more interface instability, which is controlled mostly by numerical artifacts and can result in different solutions when different numerical methods or even a different implementation is used. Observable equations remedy some of these issues by bringing down the tail of the energy spectrum.

3.2. *Detonating flow*

As mentioned for the cases of shock, turbulence, and interface, we believe that introducing additional physics such as chemical reactions over a sharp interface can add a new source for creating high-wave-mode irregularities. The addition of a reaction source term to the energy equation and the corresponding source terms to mass and momentum equations may create thin regions with high variation of flow variables. An example of such phenomena can be seen in a detonation wave where the reaction behind a detonation front transfers energy to the shock front and pushes it forward. Similar phenomena happen in deflagration when two material species react and create a new species.

The governing equation for a combustion problem, neglecting viscosity and heat diffusion, will be the nonreacting multispecies equations with the addition of a reaction

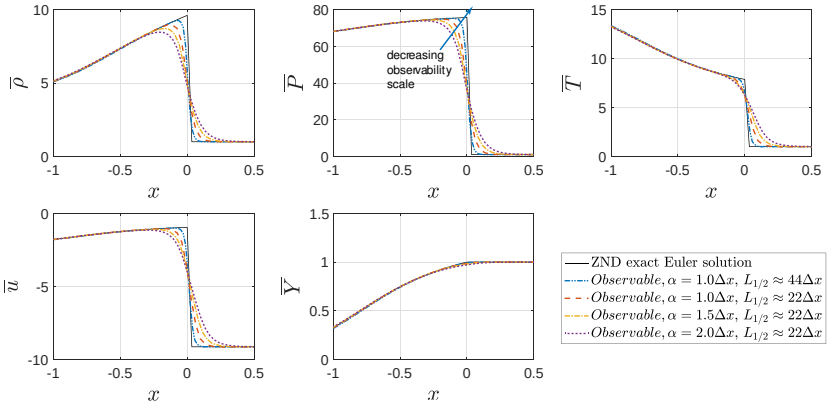

FIGURE 4. Results for a one-dimensional, steady, overdriven detonation-wave with an overdrive factor $f = 1.8$. The result for different quantities for four different simulations after reaching the steady state. As observability limit approaches zero the observable solution converges to the exact reacting Euler solution.

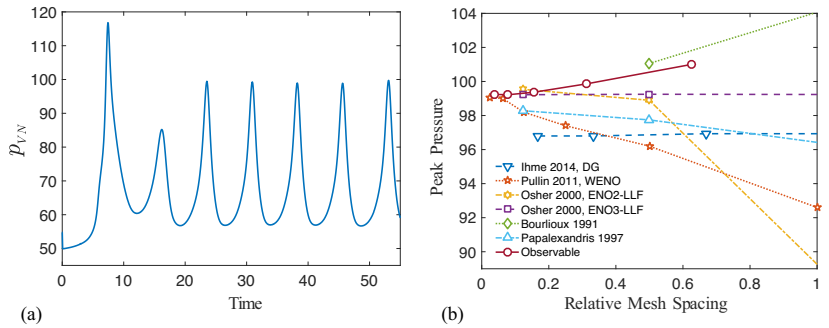

FIGURE 5. Results for a one-dimensional, unsteady, overdriven detonation-wave with an overdrive factor $f = 1.6$. (a) The von Neumann pressure over time. (b) A comparison of the peak of the von Neumann pressure for different relative mesh spacing computed by the observable method and available results from the literature (Bourlioux *et al.* 1991; Hwang *et al.* 2000; Lv & Ihme 2014; Papalexandris *et al.* 1997; Ziegler *et al.* 2011). Relative mesh spacing is $10/n_{L_{1/2}}$, where $n_{L_{1/2}} = L_{1/2}/\Delta x$.

source term, which is usually a function of temperature and species mass fraction. Instead of solving separate mass, momentum, and energy equations for each species, it is most common to solve the conservation equation for total mass, total momentum, and total energy. Additionally, for a N species reaction, it is required to solve conservation of mass for $N-1$ species in the reaction. This way, the reaction source terms appear only explicitly in the governing equation for the species' conservation of mass. The observable governing equations for the mixture properties are Eqs. (3.1)–(3.3), where the barred quantities are the observed quantities calculated with Eq. (2.1). Here, we use a Helmholtz filter as the kernel for the convolution with a length scale α. For a single-step irreversible reaction, $A \rightarrow B$, where there are only two species, an additional equation needs to be solved

$$\frac{\partial \rho Y}{\partial t} + \overline{\rho Y}\nabla \cdot \mathbf{u} + \overline{\mathbf{u}} \cdot \nabla \rho Y = \dot{\omega}, \tag{3.6}$$

where Y is the mass fraction of A and $\dot{\omega}$ is the mass production rate of species A. Ad-

ditionally, an ideal gas equation of state is used to close the system of equations. E can be written as $E = p/(\gamma - 1) + \rho u^2/2 + \rho q Y$, where γ is the ratio of specific heats and q is a heat release parameter. We study a one-dimensional overdriven detonation that has been studied extensively by other researchers to demonstrate the validity of the method. A source term with an Arrhenius form, $\dot{\omega} = -K\rho Y e^{-T_i/T}$, is used, where K is the reaction rate multiplier, T_i represents the activation energy, and T is the temperature. Here, we study the result for a one-dimensional overdriven detonation wave with two different overdrive factors $f = 1.8$ (steady detonation) and $f = 1.6$ (unsteady detonation), $T_i = 50$, and $\gamma = 1.2$. The initial condition is set following Hwang *et al.* (2000), who used a shock front with the flow variable behind the shock corresponding to the specified one-dimensional overdriven detonation wave. For this set of parameters the Chapman-Jouguet speed is $D_{CJ} = 6.8095$. All the parameters are nondimensionalized with the state variables for the unburned region. The rest of the parameters are computed following Deiterding (2003). The relevant length scale in this problem is the half reaction length, $L_{1/2}$, which is the distance behind the shock wave in which half the reactant is consumed. K is selected to be 184.6 and 230.75 for $f = 1.8$ and $f = 1.6$, respectively, in order to make $L_{1/2} = 1$. For the time integration we use a Strang splitting method to resolve the stiff reaction source term. For the time integration of the equation without a source term, we use a third order TVD Runge-Kutta, and for the solution of the ordinary differential equation including the source term, we use an analytical solution of the ordinary differential equation for simplicity. The pseudo-spectral computes all the spatial derivatives to avoid numerical dissipation and to show that the observable equations, not the numerical method, regularize the problem.

Figure 4 shows the results for one-dimensional steady overdriven detonation with $f = 1.8$. As demonstrated in the figure, the observable equations regularize the detonation front with no need for specific numerical treatment. The observable equations capture the large-scale features (far from detonation front) correctly and the observability limit decides the amount of small-scale features to retain. As shown here, as the observability limit approaches zero, the observable solution converges to the exact reacting Euler solution. The initial condition of the observable Euler is obtained by filtering the initial condition for the original Euler equation. The small effect of this inconsistency in the initial condition between the Euler and observable Euler simulations is compensated in Figure 4. In all these tests, the computed error for steady detonation front speed compared to the exact solution is less than 0.0003%.

Figure 5 shows the results for the one-dimensional overdriven detonation wave with the parameters mentioned above. Figure 5(a) demonstrates the von Neumann pressure for the unsteady detonation wave computed by the observable method with an observability limit $\alpha = 1.3\Delta x$. The von Neumann pressure is calculated by finding the shock velocity and by normal shock relations to find the pressure behind the detonation front. There is a transition time, Time < 20, before the detonation wave reaches its pulsating periodic behavior. By using the linear stability theorem (Bourlioux *et al.* 1991; Erpenbeck 1962, 1964) to study the parameters of this problem, we expect a single instability mode, which is also confirmed in the observable results. The period of oscillations as computed from our calculations converges to 7.38 as Δx and α approach zero. This is also in good agreement with the values, ranging from 7.27 to 7.49, reported by other methods solving the reacting Euler equations (Bourlioux *et al.* 1991; Deiterding 2003; Hwang *et al.* 2000; Lv & Ihme 2014; Papalexandris *et al.* 1997; Ziegler *et al.* 2011). Figure 5(b) shows the peak pressure behind the detonation wave versus relative mesh spacing, i.e., $10/n_{L_{1/2}}$, where

$n_{L_{1/2}} = L_{1/2}/\Delta x$. As shown in the figure, peak pressure computed by the observable method converges to 99.2, which is in good agreement with the values reported in the literature (Bourlioux *et al.* 1991; Deiterding 2003; Hwang *et al.* 2000; Papalexandris *et al.* 1997; Ziegler *et al.* 2011), which are approximately 99. There is a finite observability length scale in our method, and a comparison with Euler results can be misleading since the Euler solution is in fact an observable solution with a zero observability length scale. A better comparison might be made between the observable results and the experimental results or the Navier-Stokes equation, where an observability length scale is always enforced owing to the diffuse nature of the interface.

4. Conclusions

The importance of the observability limit in deriving the governing equations in continuum flows is discussed. With the introduction of observable field quantities, governing PDEs for regularized conservation laws could be derived. The essence of the approach is to realize that in any experiment or numerical simulation there is always a minimum length scale below which one cannot capture field quantity details; we call this length scale the observability length scale. We derived the observable version of Euler and Navier-Stokes equations using the observable divergence theorem. In this work we extended the observability concept to two-phase and chemical reactive flows. Results for shock-bubble interaction problems with the observable equations were demonstrated. Compared with available experimental and numerical data, the observable solution shows promising results. We also examined a one-dimensional detonation problem using the observable equations and showed that the results were in good agreement with the exact solution for the steady case and with the available data in the literature for the unsteady case. Note that all the computations in this work are performed by the pseudo-spectral method to avoid contamination of the result with any numerical dissipation. In the observable approach the regularization is done at the level of the PDE and not at the discretization level.

A few items remain to be addressed in the future. In the derivation of the observable equation for tracking a material interface, the dilatation term is neglected. This does not introduce significant error into the problems that are presented here; however, it could be important in certain problems, e.g., the bubble collapse problem. Detonation problems in two or three dimensions create new features such as triple points, which are interface curvature dependent. Observable curvature treatment could be the topic of a future investigation.

REFERENCES

Bourlioux, A., Majda, A. J. & Roytburd, V. 1991 Theoretical and numerical structure for unstable one-dimensional detonations. *SIAM J. Appl. Math.* **51**, 303–343.

Cook, A. W. & Cabot, W. H. 2005 Hyperviscosity for shock-turbulence interactions. *J. Comput. Phys.* **203**, 379–385.

Coralic, V. & Colonius, T. 2014 Finite-volume WENO scheme for viscous compressible multicomponent flows. *J. Comput. Phys.* **274**, 95–121.

Deiterding, R. 2003 Parallel adaptive simulation of multi-dimensional detonation structures. PhD thesis, Brandenburg University of Technology Cottbus.

Erpenbeck, J. J. 1962 Stability of steady-state equilibrium detonations. *Phys. Fluids* **5**, 604–614.

Erpenbeck, J. J. 1964 Stability of idealized one?reaction detonations. *Phys. Fluids* **7**, 684–696.

Gottlieb, S. & Shu, C.-W. 1998 Total variation diminishing Runge-Kutta schemes. *Math. Comput.* **67**, 73–85.

Gurbatov, S. N., Simdyankin, S. I., Aurell, E., Frisch, U. & Toth, G. 1997 On the decay of Burgers turbulence. *J. Fluid Mech.* **344**, 339–374.

Haas, J. F. & Sturtevant, B. 1987 Interaction of weak shock waves with cylindrical and spherical gas inhomogeneities. *J. Fluid Mech.* **181**, 41–76.

Hejazialhosseini, B., Rossinelli, D., Bergdorf, M. & Koumoutsakos, P. 2010 High order finite volume methods on wavelet-adapted grids with local time-stepping on multicore architectures for the simulation of shock-bubble interactions. *J. Comput. Phys.* **229**, 8364–8383.

Hou, T. Y. & Li, R. 2007 Computing nearly singular solutions using pseudo-spectral methods. *J. Comput. Phys.* **226**, 379–397.

Hwang, P., Fedkiw, R. P., Merriman, B., Aslam, T. D., Karagozian, A. R. & Osher, S. J. 2000 Numerical resolution of pulsating detonation waves. *Combust. Theor. Model.* **4**, 217–240.

Kraichnan, R. H. 1968 Lagrangian-history statistical theory for Burgers' equation. *Phys. Fluids* **11**, 265–277.

Lantz, R. 1971 Quantitative evaluation of numerical diffusion (truncation error). *Soc. Petrol. Eng. J.* **11**, 315–320.

Lv, Y. & Ihme, M. 2014 Discontinuous Galerkin method for multicomponent chemically reacting flows and combustion. *J. Comput. Phys.* **270**, 105–137.

Mohseni, K. 2009 Derivation of regularized Euler equations from basic principles. *AIAA Paper* 2009-5695.

Mohseni, K. 2010 Observable divergence theorem: evolution equations for inviscid regularization of shocks and turbulence. *arXiv preprint arXiv:1010.2612* .

Moin, P. & Apte, S. V. 2006 Large-eddy simulation of realistic gas turbine combustors. *AIAA J.* **44**, 698–708.

Norgard, G. & Mohseni, K. 2008 A regularization of the Burgers equation using a filtered convective velocity. *J. Phys. A* **41**, 344016.

Norgard, G. & Mohseni, K. 2009 On the convergence of convectively filtered Burgers equation to the entropy solution of inviscid Burgers equation. *Multiscale Model. Sim.* **7**, 1811–1837.

Norgard, G. & Mohseni, K. 2010 A new potential regularization of the one-dimensional Euler and homentropic Euler equations. *Multiscale Model. Sim.* **8**, 1212–1242.

Papalexandris, M. V., Leonard, A. & Dimotakis, P. E. 1997 Unsplit schemes for hyperbolic conservation laws with source terms in one space dimension. *J. Comput. Phys.* **134**, 31–61.

Quirk, J. J. & Karni, S. 1996 On the dynamics of a shock-bubble interaction. *J. Fluid Mech.* **318**, 129–163.

Shyue, K.-M. 1998 An efficient shock-capturing algorithm for compressible multicomponent problems. *J. Comput. Phys.* **142**, 208–242.

Ziegler, J. L., Deiterding, R., Shepherd, J. E. & Pullin, D. I. 2011 An adaptive high-order hybrid scheme for compressive, viscous flows with detailed chemistry. *J. Comput. Phys.* **230**, 7598–7630.